Met. Mater. Int., Vol. 15, No. 3 (2009), pp. 373~378
doi: 10.1007/s12540-009-0373-4 Published 26 June 2009

A Nanoindentation Study on the Micromechanical Characteristics of API X100 Pipeline Steel

Byoung-Wook Choi[1], Dong-Han Seo[2], and Jae-il Jang[1,*]

[1]Division of Materials Science and Engineering, Hanyang University,
17 Haengdang-dong, Seongbuk-gu, Seoul 133-791, Korea
[2]Technical Research Laboratories, POSCO, Pohang-si Gyeongbuk 790-785, Korea

(received date: 5 January 2009 / accepted date: 6 March 2009)

The hardness characteristics of constituent micro-phases (ferrite and bainite) in a dual-phase API X100 pipeline steel were analyzed by nanoindentation experiments. The measured nano-hardness of the bainite phase is from 3.8 GPa to 4.9 GPa, which is much higher than that of the ferrite phase, which ranged from 1.75 GPa to 2.3 GPa. With the hardness and volume fraction of each micro-phase, attempts were made to predict the overall hardness by applying a simple rule-of-mixture. A comparison between the predicted overall hardness value and the experimentally measured value revealed that the rule-of-mixture can be successfully applied for prediction purposes. The results are discussed in terms of the grain boundary strengthening effect and the indentation size effect.

Keywords: nanoindentation, hardness, pipeline steel, rule-of-mixture

1. INTRODUCTION

Given that applying higher strength pipeline steels can significantly reduce the total cost in the construction of transmission pipelines for natural gas or crucial oil [1-2], many efforts have been made to develop and apply higher grade pipeline steels beyond the widely-used API X65 steel with its yield strength of 65 ksi (~450 MPa). As a result, API X100 and even X120 grade steels are currently considered for practical use in the field [1,3-6]. The most recent challenge in this area is the development of advanced steels that are suitable for the new design concept of a pipeline (referred to as a "strain-based design pipeline," i.e., a pipeline applicable to seismic and permafrost regions where large plastic deformation can be introduced) [7,8]. This strain-based design pipeline steel requires excellent deformability (high work-hardening ability) in addition to a high strength. As dual-phase microstructures consisting of hard and soft phases are known to have higher hardenability compared to single-phase structures [4,9,10], two types of microstructures have been extensively considered for high-deformability pipeline steels: ferrite-bainite and bainite-martensite microstructures. To develop such a dual-phase steel, optimization of the volume fraction of each constituent phase is essential to obtain proper target properties because each individual phase can competitively affect the overall properties of the steel [11,12]. In this regard, it is very important to understand the basic mechanical properties (or behavior) of each constituent micro-phase.

Over the past decade, nanoindentation [13,14] has been widely used to probe the mechanical properties of very small volumes in a material. Using this technique, various efforts have been made to measure microstructures hardness, elastic modulus and other mechanical properties of micro-phases in multi-phase steels and composite materials [15-22]. In a similar vein, the micromechanical characteristics of dual-phase API X100 pipeline steel (having a microstructure consisting of ferrite and bainite) are analyzed in the present study through nanoindentation experiments. The investigation consists of two parts: First, the nanoindentation hardness of each micro-phase is characterized. Subsequently, with the measured hardness and volume fraction of each phase, the overall hardness of the steel is predicted by applying a simple rule-of-mixture (which is commonly used to analyze the strength properties of composite and multiphase materials [23-25]). From engineering viewpoints, the prediction of the overall hardness from the phase hardness may be helpful in improving the design of high-performance dual-phase (or multi-phase) steel through optimization of the volume fraction of the constituent phases.

*Corresponding author: jijang@hanyang.ac.kr

Table 1. Chemical composition and carbon equivalent (C_{eq}) of the examined API X100 steel

Elements	C	Si	Mn	P	S	Nb	V	Mo	Ceq
Content (%)	0.05~0.07	0.25	≤ 2.0	≤ 0.01	≤ 0.001	≤ 0.05	≤ 0.05	≤ 0.3	0.46~0.48

2. EXPERIMENTAL PROCEDURE

The material examined here is API-X100 grade high-strength pipeline steel fabricated by a thermo-mechanical controlled process (TMCP). The chemical composition and carbon equivalent of the steel are listed in Table 1. The samples were taken from a 19.5-mm-thick plate. Figure 1 presents a representative scanning electron microscopy (SEM) image showing the microstructure of the steel. As seen in the figure, the microstructure mainly consists of the dual phases of ferrite and bainite. The grain size of the ferrite phase is 3 μm to 9 μm, while the bainite phase is subdivided into very fine laths. The tensile tests (made primarily of plate-bar-type specimens taken along the rolling direction) revealed that the yield strength and tensile strength of the material are 680 MPa and 850 MPa, respectively.

Nanoindentation tests were carried out using a Nanoindenter-XP equipment (Nano Instruments Inc., Oak Ridge, TN, USA) with a three-sided pyramidal Berkovich tip. The load-controlled experiments were performed up to a maximum load (P_{max}) of 5 mN at a constant strain rate of 0.05/s. More than 5 indentation tests under each testing condition were made on an electro-polished sample as opposed to a mechanically polished sample in order to avoid experimental artifacts related to the hardened surface layer. The specimen surface was initially ground and then electro-chemically polished using a Lectropol-5 instrument (Struers, Westlake, OH, USA) in a solution appropriate for steel (butoxy-ethanol 35 %, methanol 59 % and perchloric acid 6 %) at -30 °C.

After the nanoindentation test, the specimens were slightly etched in 3 % nital acid and the hardness impression and microstructure were observed via field-emission SEM, JSM-6330F (Jeol Ltd., Tokyo, Japan) to determine whether or not an indentation was made inside the target micro-phase. The volume fraction of each phase was measured by an image analyzer, Image-Pro (Media Cybernetics Inc., Silver Spring, MD, USA). For comparison with the predicted overall hardness, Vickers hardness tests were also carried out with a HMV-2 tester (Shimadzu Inc., Kyoto, Japan).

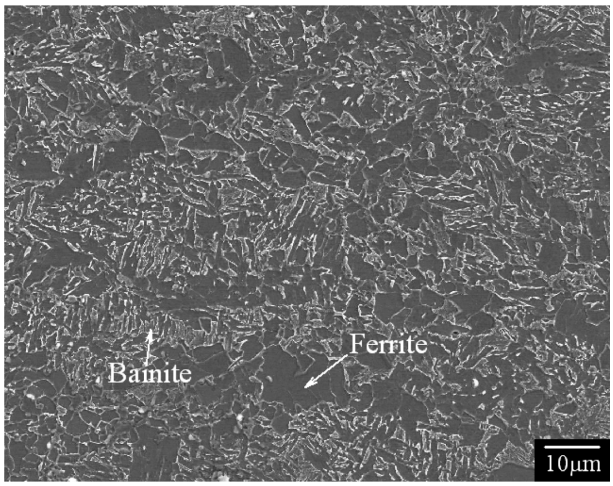

Fig. 1. Scanning electron micrograph showing the typical microstructure of API X100 steel examined in the present work.

3. RESULTS AND DISCUSSION

Figure 2 shows representative examples of load-displacement (*P-h*) curves recorded during a nanoindentation made at P_{max} = 5 mN. These experiments were performed at three different positions throughout the thickness (t = 19.5 mm), i.e., t/2, t/4, and t/8, in order to assess any possible through-thickness variation in the strength. It is apparent in the figure that, for all three positions, the ferrite phase exhibits a much larger peak-load displacement compared to that of the bainite phase, implying that the former phase is much softer than the latter phase. It is also notable that an indentation on a target phase could not be intentionally made because the tests were done on an electro-polished surface. Thus, after slightly etching the indented surface, the hardness impression and microstructure were observed again by SEM, which made it possible to select the indentations made within a target phase (see inset images of Fig. 2).

The measured nanoindentation hardness (termed the nano-hardness) values are summarized in Fig. 3. The fluctuation in the nano-hardness of the micro-phase may be related to the hardness dependency on the intrinsic characteristics of each grain, including the crystallographic orientation and the non-uniformity of the dislocation density. Nevertheless, the average hardness of each phase did not vary significantly with the through-thickness position. The hardness of the ferrite phase was 1.75 GPa to 2.3 GPa, whereas that of bainite was 3.8 GPa to 4.9 GPa. It is informative to compare these hardness values with those in the literature, although a direct comparison of the hardness is not easy due to the differences in chemical compositions of the tested steel. Choi *et al.* [15] and Delincé *et al.* [18] reported independently that the ferrite phase (having a grain size similar to that in this work - about 10 μm) has a hardness of 2 GPa to 2.5 GPa; Wu *et al.* [25] demonstrated that the hardness of bainite phase is approximately 4.3 GPa. These values in the literature are in reasonably good agreement with the present results. On the other hand, Furnémont *et al.* [26] reported much higher hardness

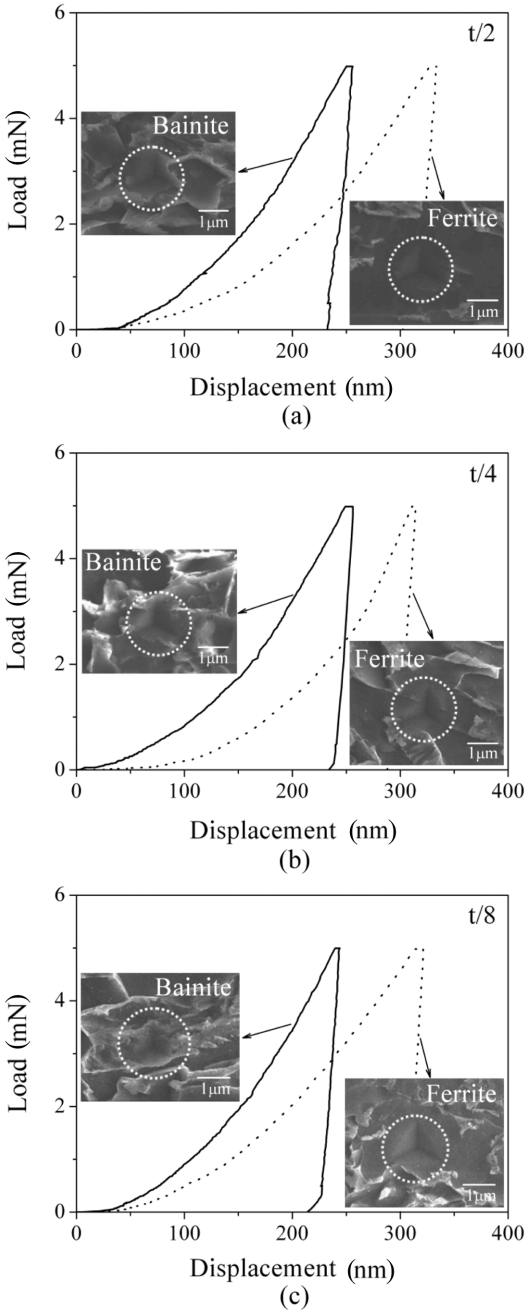

Fig. 2. Representative *P-h* curves recorded during nanoindentations of each micro-phase: (a) t/2 position, (b) t/4 position, and (c) t/8 position.

values of bainite and ferrite (4.8 GPa and 7 GPa respectively). This was possibly due to much higher carbon content in their steels (up to 0.29 %) compared to that in this work.

To predict the macroscopic overall hardness of the dual-phase steel from the nano-hardness of each phase, the applicability of a simple-of-mixture was assessed as shown below.

$$H_{total} = H_f V_f + H_b V_b \quad (1)$$

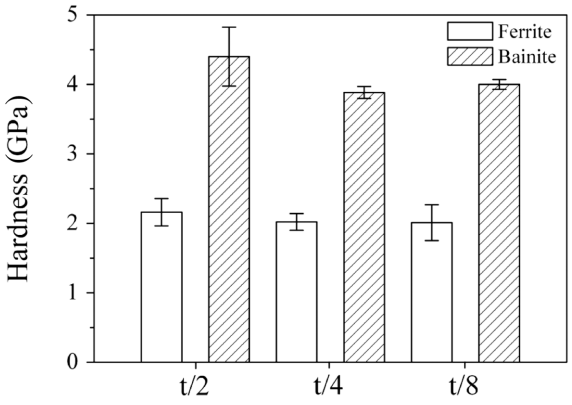

Fig. 3. Average and standard deviation of the measured nano-hardness values of the constituent phases.

Here, H is the hardness, V denotes the volume fraction, and the subscripts f and b represent the ferrite and bainite, respectively.

The volume fraction was determined as follows. First, a scratch mark was introduced, and a SEM image of the region near the scratch was taken before the indentation was made (Figs. 4(a), (b), and (c)). Near the scratch, nanoindentation tests were carried out at a very high load (P_{max} = 500 mN) and SEM images of the hardness impressions were obtained (Figs. 4(d), (e), and (f)). To estimate the volume fraction of each phase within the indentation-induced plastic zone (which should be larger than the triangular impression area), here the plastic zone was assumed to be a circle passing three (or at least two) angular points of the triangular impression. Although the actual plastic zone may be larger than this circular zone according to a number of earlier works (e.g., Johnson's expanding cavity model for elastic-plastic indentation with a cone [27]), the simple assumption mentioned above was adopted for three reasons: (1) no established means of estimating the plastic zone size precisely exists; (2) the area 'fraction' of the phase may not vary significantly with a small change in the 'size' of the plastic zone; and (3) with this assumption, a reproducible calculation of the plastic zone size becomes easier. Next, by making the SEM images transparent and then superposing one on the other based on the location of the scratch, each position in the images taken before the indentation (Figs. 4(a), (b), and (c)) could be compared directly with those after the indentation (Figs. 4(d), (e), and (f)). This made it possible to obtain the microstructural features within the circular plastic zone that was drawn in the SEM image taken before the indentation (see the circles in Figs. 4(a), (b), and (c)). Lastly, the area (and thus the volume) fraction of each phase within the circular area of the plastic zone was calculated using an image analyzer. Figures 4(g), (h), and (i) present the analyzed images in which the white and black areas correspond to the ferrite and bainite phase, respectively. The calculated volume fraction of the

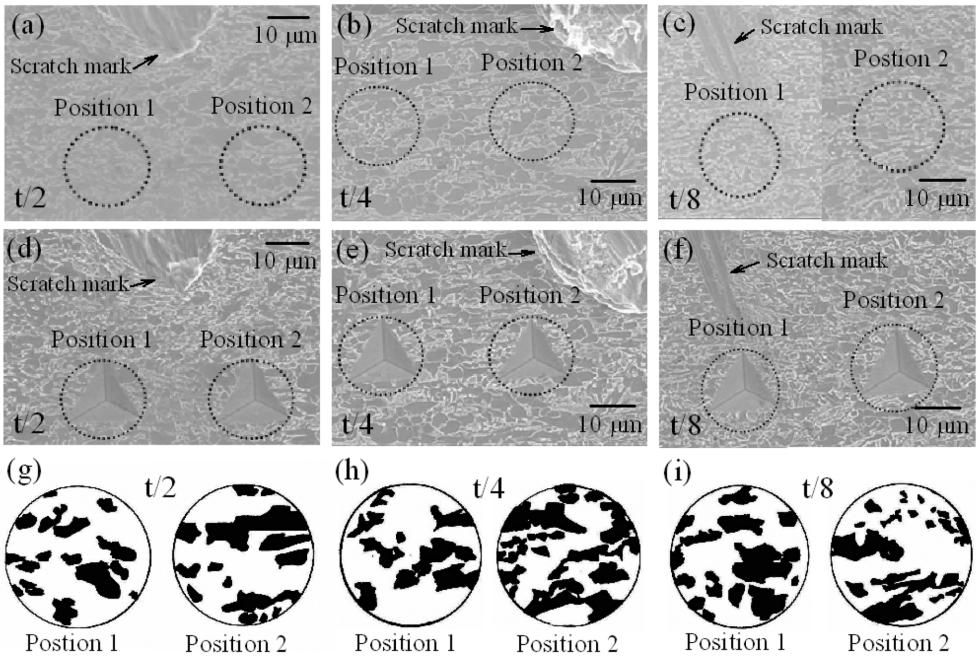

Fig. 4. Images used for applying a rule-of-mixture to the prediction of overall hardness from phase hardness: (a), (d), (g) t/2 position, (b), (e), (h) t/4t position, and (c), (f), (i) t/8t position.

bainite phase (V_b) was 0.369 and 0.254 for position 1 and 2, respectively, in the t/2 region; 0.313 and 0.504 for position 1 and 2 in the t/4 region, respectively; and 0.326 and 0.392 for position 1 and 2 in the t/8 region, respectively. The volume fraction of ferrite (V_f) could be simply calculated as (1-V_b).

The hardness values directly measured by a high load nanoindentation were compared with the hardness predicted by the rule-of-mixture (Eq. 1), which is summarized in Fig. 5. The H_f and H_b values that were applied are the average values of the measured phase hardness (summarized in Fig. 3); i.e., 2.16 GPa and 4.4 GPa for t/2, 2.02 GPa and 3.88 GPa for t/4, and 2.02 GPa and 4 GPa for t/8. In the figure, the difference between the predicted value and the experimentally measured value is reasonably small (within 0.2 GPa). This suggests that the rule-of-mixture can be successfully applied to estimate the overall hardness from the phase hardness.

For reconfirmation purposes, macroscopic Vickers hardness tests were performed at a much higher load (~28.8 N). Figure 6 shows optical micrographs taken before and after the Vickers indentation. From the micrographs, the volume fraction of each phase in the indentation-induced plastic zone was evaluated in the same manner described above (see Fig. 7). Figure 8 summarizes both the macroscopic hardness directly measured by the Vickers hardness tests and the hardness predicted by Eq. 1. In the figure, for a direct comparison with the aforementioned hardness, the conventional Vickers hardness HV (defined as the maximum indentation load divided

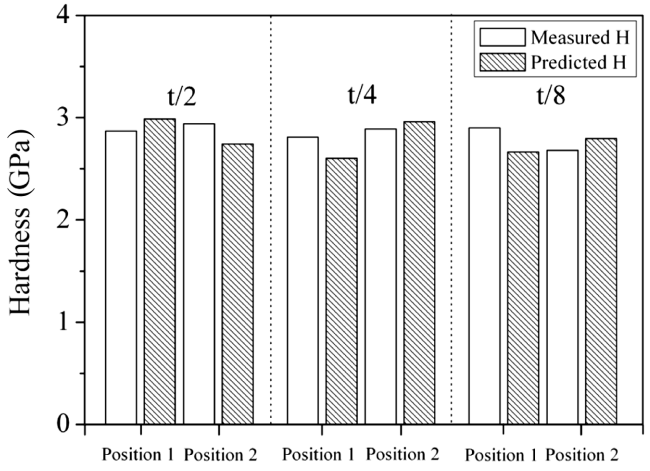

Fig. 5. Comparison of the measured hardness (at P_{max} = 500 mN) and the predicted hardness.

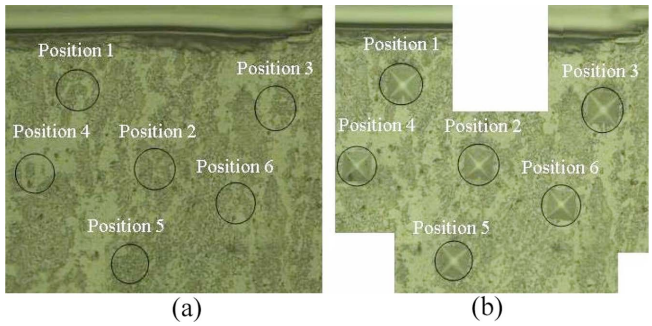

Fig. 6. Optical micrographs taken (a) before and (b) after the Vickers hardness tests.

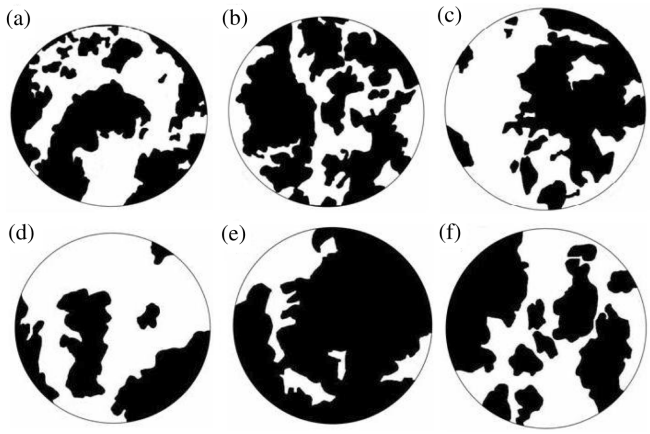

Fig. 7. Analyzed images showing the distribution of each phase: (a) to (f) correspond to positions 1 to 6 in Fig. 6.

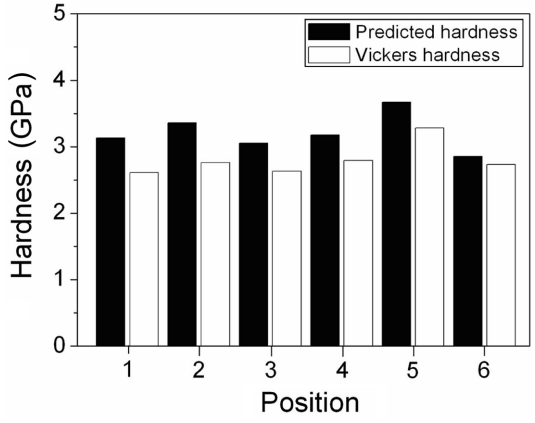

Fig. 8. Comparison of the measured hardness (at P_{max} = 28.8 N) and the predicted hardness.

by the 'surface area' of the indentation, A_S, in units of kg_f/mm^2) was converted to the indentation hardness, H, which is equal to the mean contact pressure under the indenter (i.e., the peak load divided by the 'projected area' of the indentation, A_P). The conversion process is simply given as

$$HV = \frac{P_{max}}{A_S} = \frac{2(\sin\Psi)P_{max}}{d^2} = \left(\frac{P_{max}}{A_P}\right)\sin\Psi = H\sin\Psi \quad (2)$$

where d is the Vickers indentation diagonal and Ψ is the included half-angle of the Vickers indenter (i.e. $Y = 68°$). The difference between the measurement and the prediction in Fig. 8 is slightly larger than that in Fig. 5. However, considering that the volume fraction measurements for Fig. 8 were roughly made using only optical micrographs, this difference is acceptable.

The successful prediction of the overall hardness by a simple rule-of-mixture was somewhat surprising because the phase hardness was obtained from an indentation made within a grain (see Fig. 2); accordingly, the grain boundary strengthening effect was not included in the application of the rule. Recently, Jang *et al*. [28] experimentally demonstrated that high angle boundaries play an important role in deformations during nanoindentations of structural steels. Additionally, Gong *et al.* [23] suggested that consideration of the grain size effect (i.e., boundary strengthening effect) is necessary to predict the hardness of a composite material properly when applying the rule-of-mixture. This suggests that the predicted hardness should be considerably lower than the measured hardness.

This controversy may conceivably be explained by an important phenomenon often observed in indentation experiments, namely indentation size effect (ISE), i.e., hardness increases with decreasing indentation depth (and the peak load) for a sharp indenter [29-32]. This phenomenon is known to arise from strain gradient plasticity under the indenter [29-30]. In this work, the nanoindentations made to measure the phase hardness were made at a relatively low load P_{max} = 5 mN, while the tests for evaluating the overall hardness were performed at P_{max} = 500 mN (for nanoindentation) and 28.8 N (for Vickers indentation). Assuming that the size of each phase is sufficiently large so that the indentation at P_{max} = 500 mN (or 28.8 N) can be made within a single grain, the phase hardness measured at such high loads should be much lower than the phase hardness obtained at P_{max} = 5 mN. Accordingly, the microscopic phase hardness from low-load indentation can be overestimated if compared with the macroscopic phase hardness. Collectively, the possible underestimation of the predicted overall hardness (stemming from a disregard of grain boundary strengthening in the rule-of-mixture application) may be counterbalanced (and hence overcome) by the overestimation of the phase hardness measured at a low load (due to the presence of the ISE). For a more precise prediction of the macroscopic strength from a nanoindentation, quantitative analyses of both effects (the ISE vs. the boundary strengthening effect) are desirable. These are currently underway.

From the results above, another concept is also applicable to industrial fields. If nano-hardness values of the microphases are provided, it may be possible to predict the volume fraction of each phase 'roughly' by performing a macroscopic indentation without observation of the microstructure. However, it should be noted that this inverse analysis for the prediction of the volume fraction is relatively difficult in a quantitative approach because the possible variation range of the volume fraction is much wider than that of the hardness. For instance, if V_b in Eq. 1 increases from approximately 1 % (i.e., V_f is 99 %) to 100 %, the hardness (in the case of t/2) increases from a value close to 2.16 GPa (ferrite-only hardness) to 4.4 GPa (bainite-only hardness). Thus, the increase in the hardness (by approximately 2 times) cannot sensitively reflect the dramatic increase in the volume fraction (100 times).

4. CONCLUSION

Nanoindentation experiments were performed to evaluate the nano-hardness of micro-phases (bainite and ferrite) in dual-phase API X100 pipeline steel. With the nano-hardness of each phase, successful prediction of the overall hardness was possible by applying a simple rule-of-mixture. These successful predictions occur possibly due to the counterbalance between the potential underestimation of the predicted overall hardness (related to disregard of the boundary strengthening effect) and the overestimation of the phase hardness measured at a low load (due to the ISE).

ACKNOWLEDGMENT

This work was sponsored by POSCO.

REFERENCES

1. N. Sanderson, R. K. Ohm, and M. Jacobs, *Oil Gas J.* **97**, 54 (1999).
2. K. T. Corbett, R. R. Bowen, and C. W. Peterson, *Proceeding of 13th International Offshore and Polar Engineering Conference*, p. 105, The International Society of Offshore and Polar Engineers, Hawaii, USA (2003).
3. A. Glover, J. Zhou, D. Horsley, N. Suzuki, S. Endo, and J. Takehara, *Proceeding of 22nd International Conference on Offshore Mechanics and Arctic Engineering*, Art. No. OMAE2003-37429, American Society of Mechanical Engineers, Cancun, Mexico (2003).
4. N. Ishikawa, M. Okatsu, S. Endo, and J. Kondo, *Proceeding of 6th International Pipeline Conference*, Art. No. IPC2006-10240, American Society of Mechanical Engineers, Calgary, Canada (2006).
5. N. Ishikawa, S. Endo, and J. Kondo, *JFE Technical report* **7**, 20 (2006).
6. D.-H. Seo, C.-M. Kim, J.-Y. Yoo, and K.-B. Kang, *Proceeding of 17th International Offshore and Polar Engineering Conference*, p. 3301, The International Society of Offshore and Polar Engineers, Hawaii, Lisbon, Portugal (2007).
7. N. Suzuki and M. Toyoda, *Proceeding of 21st International Conference on Offshore Mechanics and Arctic Engineering*, Art. No. OMAE2003-28253, American Society of Mechanical Engineers, Oslo, Norway (2002).
8. N. Suzuki, R. Muraoka, A. Glover, J. Zhou, and M. Toyoda, *Proceeding of 22nd International Conference on Offshore Mechanics and Arctic Engineering*, Art. No. OMAE2003-37145, American Society of Mechanical Engineers, Cancun, Mexico (2003).
9. S. Endo and M. Nagae, *ISIJ Int*. **36**, 95 (1996).
10. T. Hüper, S. Endo, N. Ishikawa, and K. Osawa, *ISIJ Int*. **39**, 288 (1999).
11. M. Taya and R. J. Arsenault, *Metal Matrix Composites: Thermo-mechanical Behavior*, Pergamon Press, NY (1989).
12. N. Chawla and K. K. Chawla, *Metal Matrix Composite*, Springer, NY (2006).
13. W. C. Oliver and G. M. Pharr, *J. Mater. Res*. **7**, 1564 (1992).
14. J. L. Hay and G. M. Pharr, *Instrumented Indentation Testing*, ASM Handbook, OH, p. 232, (2000).
15. Y. Choi, W. Y. Choo, and D. kwon, *Scripta mater.* **45**, 1401 (2001).
16. N. X. Randall, C. Julia-Schmutz, J. M. Soro, J. von Stebut, and G. Zacharie, *Thin Solid Films* **308-309**, 297 (1997).
17. P. J. Jacque, Q. Furnémont, F. Lani, T. Pardoen, and F. Delannay, *Acta mater.* **55**, 3681 (2007).
18. M. Delincé, P. J. Jacques, and T. Pardoen, *Acta mater.* **54**, 3395 (2006).
19. H. Bei, E. P. George, and G. M. Pharr, *Mater. Sci. Eng. A* **483-484**, 218 (2008).
20. L. Han, H. Hu, D. O. Northwood, and N. Li, *Mater. Sci. Eng. A* **473**, 16 (2008).
21. Y. Sun, J. Liang, Z.-H Xu, G. Wang, and X. Li, *J. Mater. Sci.* **19**, 514 (2008).
22. B.-W. Choi, D.-H. Seo, J.-Y. Yoo, and J.-I. Jang, *J. Mater. Res* **24**, 816 (2009).
23. J. Gong, H. Miao, and B. Hu, *Mat. Sci. Eng. A* **372**, 207 (2004).
24. T. Ohmura, K. Sawada, K. Kimura, and T. Suzaki, *Mat. Sci. Eng. A* **489**, 85 (2008).
25. K. Wu, Z. Li, A. M. Guo, X. He, L. Ahang, A. Fang, and L. Cheng, *ISIJ Int.* **46**, 161 (2006).
26. Q. Furnémont, M. Kempf, P. J. Jacques, M. Goken, and F. Delannay, *Mat. Sci. Eng. A* **328**, 26 (2002).
27. K. L. Johnson, *J. Mech. Phys. Solids* **18**, 115 (1970).
28. J. -I. Jang, S. Shim, S. Komazaki, and T. Honda, *J. Mater. Res.* **22**, 175 (2007).
29. W. D. Nix and H. Gao, *J. Mech. Phys. Solids* **46**, 411 (1998).
30. J. G. Swadener, E. P. George, and G. M. Pharr, *J. Mech. Phys. Solids* **50**, 681 (2002).
31. J.-Y. Kim, S.-K. Kang, J.-J. Lee, J.-I. Jang, Y.-H. Lee, and D. Kwon, *Acta mater.* **55**, 3555 (2007).
32. J.-Y. Kim, S.-H. Kim, J.-S. Lee, K.-W. Lee, and D. Kwon, *Met. Mater. Int*. **12**, 219 (2006).